Tubular Surface Evolution for Segmentation of the Cingulum Bundle From DW-MRI

Vandana Mohan, Ganesh Sundaramoorthi, John Melonakos, Marc Niethammer, Marek Kubicki, Allen Tannenbaum

Tubular Surface Evolution for Segmentation of the Cingulum Bundle From DW-MRI

Vandana Mohan[1], Ganesh Sundaramoorthi[2], John Melonakos[1], Marc Niethammer[3], Marek Kubicki[4], and Allen Tannenbaum[1]

[1] Georgia Institute of Technology, Atlanta, GA, USA
[2] University of California, Los Angeles, CA, USA
[3] University of North Carolina, Chapel Hill, NC, USA
[4] Brigham Women's Hospital, MA, USA
gth115a@mail.gatech.edu

Abstract. This work provides a framework for modeling and extracting the Cingulum Bundle (CB) from Diffusion-Weighted Imagery (DW-MRI) of the brain. The CB is a tube-like structure in the brain that is of potentially of tremendous importance to clinicians since it may be helpful in diagnosing Schizophrenia. This structure consists of a collection of fibers in the brain that have locally similar diffusion patterns, but vary globally. Standard region-based segmentation techniques adapted to DW-MRI are not suitable here because the diffusion pattern of the CB cannot be described by a *global* set of simple statistics. Active surface models extended to DW-MRI are not suitable since they allow for arbitrary deformations that give rise to unlikely *shapes*, which do not respect the tubular geometry of the CB. In this work, we explicitly model the CB as a tube-like surface and construct a general class of energies defined on tube-like surfaces. An example energy of our framework is optimized by a tube that encloses a region that has *locally* similar diffusion patterns, which differ from the diffusion patterns immediately outside. Modeling the CB as a tube-like surface is a *natural shape prior*. Since a tube is characterized by a center-line and a radius function, the method is reduced to a 4D (center-line plus radius) curve evolution that is computationally much less costly than an arbitrary surface evolution. The method also provides the center-line of CB, which is potentially of clinical significance.

1 Introduction

In this work, we are interested in extracting a structure in the brain called the *cingulum bundle* (CB) from *diffusion-weighted magnetic resonance imagery (DW-MRI)* of the brain. DW-MRI is imagery that at each voxel indicates the diffusion of water molecules at each particular sampling *direction* in $3D$ space. Adding an extra dimension, directionality, to the data is necessary to discriminate our structure of interest - the cingulum bundle. The CB has recently become the subject of interest as an anatomical structure which may display quantifiable differences between schizophrenic and normal control populations, and studying it may aid in the diagnosis of schizophrenia [1, 2].

The Cingulum Bundle is a *thin, highly curved* structure that consists of a collection of neural fibers, which are mostly disjoint possibly intersecting, roughly aligned

and centered around a fiber. The collection of fibers approximately form a tube-like structure. The diffusion pattern in the CB varies in orientation and anisotropy smoothly along the structure, and it has a distinct diffusion pattern from surrounding areas of the brain (see Fig. 2 for a sagittal slice of the CB). The CB possesses a challenge to segment because of inhomogeneity of its diffusion pattern *globally* and the noisy nature of DW-MRI makes it difficult to detect edges separating the CB from the rest of the image.

There has been much research in detecting and characterizing neural connections between brain structures in DW-MRI. Early methods for detecting fibers, i.e., *tractography*, are based on streamlines where the fiber path is constructed by following the direction of the principal eigenvector of diffusion tensors from an initial seed point, e.g., [3, 4]. These methods have been shown to perform poorly in noisy situations and they often terminate prematurely before the fiber ending. To alleviate these problems, there has been a number of works, e.g., [5–11], where an optimal path, in some sense, is constructed from seed region(s). The procedure is repeated to detect all fibers of a bundle. These methods, however, do not explicitly provide a segmentation of the entire fiber bundle.

We are interested in segmenting the entire fiber bundle as a surface. Standard active surface techniques, e.g. [12, 13], adapted to DW-MRI are typically difficult to segment the CB since the DW-MRI of the brain are extremely noisy and contain many local features that trap the active surface in unlikely configurations that are not representative of the CB. Indeed, the CB is difficult to segment without a *shape prior* favoring its thin tube-like geometry. Standard region-based techniques adapted to DW-MRI or DT-MRI, e.g. [14], are generally not applicable to the segmentation of the CB since the statistics of the DW-MRI inside the CB cannot be described by a few *global* parameters (e.g. mean). The Mumford-Shah energy extended to DT-MRI, [15], which assumes piecewise smooth image data inside the surface, is applicable to the CB, but the technique needs a shape prior for the CB and is computationally costly since smooth functions must be determined at each update of the evolving surface. In [16], the authors model the probability distribution of the CB and design an algorithm to classify voxels of the image, and the method could benefit greatly modeling the CB geometry. Noticing that standard region-based techniques are not applicable to the CB, an edge-based active surface method for segmenting the CB is considered by [17]. However, the method is sensitive to the noise in the DW-MRI, and the method does not incorporate the tube-like geometry into the segmentation. The work [18] designs an energy on volumetric regions that incorporates "local region-based" information and a prior favoring regions that are close to an initially detected center-line curve. However, the energy is highly dependent on the correct placement of the detected center-line, which is often not exactly in the center of the CB. Moreover, the method does not enforce the tube-like geometry of the CB.

In this work, *we explicitly model the CB as a tubular surface*, and *construct a general class of energies defined on these tubular surfaces*. This enforces a tubular geometry during the segmentation process. Since the tubular surfaces we consider are determined by a center-line in 3D space and a radius function defined at each point of the center-line (see Fig. 1), the problem is reduced to optimizing an energy defined on 4D curves. *This significantly reduces the computational cost of the optimization proce-*

dure when compared to an unconstrained surface optimization. Further, *we show how to construct energies that are tailored to the varying nature of the diffusion pattern in the CB*.

Our method is inspired by the work of [19] in which the authors model vessels as tubular regions formed by the union of spheres along a center-line. Energies are constructed on 4D curves that represent tubes, and these energies are globally minimized using the minimal path technique [20]. The energies we construct cannot be optimized using the minimal path technique since our energies are directionally dependent - they depend on the position of the 4D curve and its *tangent*. Moreover, for the energies we consider, we are not interested in a global minimum but rather certain local minima. As we shall see (in Section 4), the optimization of our energy of interest using gradient descent requires special consideration, and this interestingly ties to the metric structure on the space of 4D curves.

2 The Cingulum Bundle

The cingulum bundle is a 5-7 mm in diameter fiber bundle that interconnects all parts of the limbic system. It originates within the white matter of the temporal pole, and runs posterior and superior into the parietal lobe, then turns, forming a "ring-like belt" around the corpus callosum, into the frontal lobe, terminating anterior and inferior to the genu of the corpus callosum in the orbital-frontal cortex [21]. Moreover, the CB consists of long, association fibers that directly connect temporal and frontal lobes, as well as shorter fibers radiating into their own gyri. The CB also includes most afferent and efferent cortical connections of cingulate cortex, including those of prefrontal, parietal and temporal areas, and the thalamostriatae bundle. In addition, lesion studies document a variety of neurobehavioral deficits resulting from a lesion located in this area, including akinetic mutism, apathy, transient motor aphasia, emotional disturbances, attentional deficits, motor activation, and memory deficits. Because of its involvement in executive control and emotional processing, the CB has been investigated in several clinical populations, including depression and schizophrenia. Previous studies, using DTI, in schizophrenia, demonstrated decrease of FA in anterior part of the cingulum bundle [1, 2], at the same time pointing to the technical limitations restricting these investigations from following the entire fiber tract.

3 Proposed Framework

In this section, we model the cingulum bundle (CB) as a tubular surface in $\mathbb{R}^3$. We show that the tubular surface is completely determined by its center-line and the radius function of the discs along the center-line, and therefore, the tubular surface in $\mathbb{R}^3$ can be effectively reduced to a curve in $\mathbb{R}^4$. We formulate a general class of energies directly on curves living in $\mathbb{R}^4$, and then observe that special consideration of the metric structure on curves is needed to optimize the energy.

3.1 Modeling the Cingulum Bundle (CB) as a Tubular Surface

We are interested in tubular surfaces since these surfaces naturally model the CB. These surfaces have the additional advantage that they may be represented as space curves thus significantly reducing the computational complexity of our algorithm.

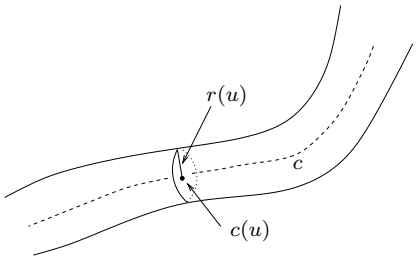

Fig. 1. Illustration of Tubular Surface model

The tubular surfaces we consider are determined by a center line, which is an open curve lying in $\mathbb{R}^3$, and a radius function defined at each point of the center-line. Given an open curve $c : [0,1] \to \mathbb{R}^3$, the center line, and a function $r : [0,1] \to \mathbb{R}^+$, the radius function, we can define the tubular surface, $S : \mathbb{S}^1 \times [0,1] \to \mathbb{R}^3$ ($\mathbb{S}^1$ is $[0, 2\pi]$ with endpoints identified) as follows:

$$S(\theta, u) = c(u) + r(u)[n_1(u)\cos\theta + n_2(u)\sin\theta] \tag{1}$$

where $n_1, n_2 : [0,1] \to \mathbb{R}^3$ are normals to the curve c defined to be orthonormal, smooth, and such that the dot products $c'(u) \cdot n_i(u)$ vanish. See Fig. 1 for an illustration of a tubular surface. The idea is simply that the tubular surface is represented as a collection of circles each of which lie in the plane perpendicular to the center line. Note that the surface in (1) may thus be identified with a 4D space curve, $\tilde{c} : [0,1] \to \mathbb{R}^4$, defined as a cross-product:

$$\tilde{c}(u) = (c(u), r(u))^T. \tag{2}$$

3.2 Variational Approach for Detecting the Cingulum Bundle

We now define a general class of energy functionals defined directly on 4D curves (2) that when optimized result in the 4D curve that represents the CB from DW-MRI of the brain.

Let $\mathbb{S}^2 \subset \mathbb{R}^3$ denote the 2D sphere, which is to represent the set of all possible angular acquisition directions of the scanning device for DW-MRI. Let $I : \mathbb{R}^3 \times S^2 \to \mathbb{R}^+$ be the diffusion image. We are interested in weighted length functionals on 4D curves as energy functionals of interest. Indeed, let $\Psi : \mathbb{R}^4 \times S^2 \to \mathbb{R}^+$ ($\Psi(x, r, v) \in \mathbb{R}^+$) be a weighting function, which we call the *potential* to be chosen, and define the energy as

$$E(\tilde{c}) = \int_{\tilde{c}} \Psi(\tilde{c}(\tilde{s}), \frac{c'(\tilde{s})}{|c'(\tilde{s})|})\, \mathrm{d}\tilde{s},\ \ \tilde{c} = (c, r) \tag{3}$$

where $\mathrm{d}\tilde{s} = |\tilde{c}'(u)|\,\mathrm{d}u = \sqrt{(r'(u))^2 + |c'(u)|^2}\,\mathrm{d}u$ is the arclength measure of the 4D curve, and $c'(\tilde{s})/|c'(\tilde{s})|$ is the unit tangent to c, the center line. When (3) is minimized, the term $\mathrm{d}\tilde{s}$ penalizes the non-smoothness of the center line and the radius function. The energy (3) is related to the length of a curve in a Finsler manifold [22].

The goal is to choose Ψ so that the energy is optimized by a $\tilde{c}$ which determines a surface enclosing the diffusion pattern of the CB in the DW-MRI of the brain. The diffusion pattern in the cingulum varies in orientation and anisotropy across the length of the bundle, although *locally* similar (see Fig. 2), and that pattern differs from the pattern immediately outside the CB. This fact precludes the use of traditional region-based techniques adapted to DT-MRI since these techniques assume homogeneous statistics within the *entire* region enclosed by the surface, whereas we will assume homogeneity within local regions. In the next section, we show how Ψ may be chosen so that the energy can capture the varying diffusion pattern of the CB. The idea is to choose Ψ at a particular coordinate (x, r, p) to incorporate statistics of the DT-MRI *local* to the disc determined by (x, r, p) rather than using statistics global to the entire structure as in traditional region based methods.

3.3 Example Potentials, Ψ

In this section, we give two choices of Ψ that are meaningful for extracting the CB from DW-MRI, both based on *local* region-based statistics.

The first potential Ψ_1 at a coordinate $(x, r, v) \in \mathbb{R}^3 \times \mathbb{R}^+ \times \mathbb{S}^2$ is constructed so as to be small when the *mean diffusion profile* inside the disc, $D(x, r, v)$, differs greatly from the mean diffusion profile inside the annular region, $D(x, \alpha r, v) \backslash D(x, r, v)$ where $\alpha > 1$, outside $D(x, r, p)$. This is given by the following expressions:

$$\Psi_1(\tilde{p}, v) = \frac{1}{1 + \|\mu_{D(\tilde{p},v)} - \mu_{D((p,\alpha r),v)\backslash D(\tilde{p},v)}\|^2} \tag{4}$$

where the μ's are means:

$$\mu_{D(\tilde{p},v)}(\hat{v}) = \frac{1}{r^2} \int_{D(\tilde{p},v)} I(x, \hat{v}) \, \mathrm{d}A(x) \tag{5}$$

$$\mu_{D((p,\alpha r),v)\backslash D(\tilde{p},v)}(\hat{v}) = \frac{1}{(\alpha^2 - 1)r^2} \int_{D((p,\alpha r),v)\backslash D(\tilde{p},v)} I(x, \hat{v}) \, \mathrm{d}A(x), \tag{6}$$

where $\mathrm{d}A$ is the area element and $\| \cdot \|$ is a suitable norm on functions of the form $f : \mathbb{S}^2 \to \mathbb{R}^+$, e.g.,

$$\|f_1 - f_2\|^2 = \int_{\mathbb{S}^2} |f_1(v) - f_2(v)|^2 \, \mathrm{d}S(v), \tag{7}$$

where $\mathrm{d}S$ is the surface area element. The energy corresponding to Ψ_1 is *minimized*.

Another example potential is chosen such that the corresponding energy is related to a weighted surface area:

$$\Psi_2(x, r, p) = r \int_0^{2\pi} \phi(x + r p^{\perp}(\theta)) \, \mathrm{d}\theta, \text{ and } p^{\perp}(\theta) = n_1 \cos\theta + n_2 \sin\theta \tag{8}$$

where n_1, n_2 are orthonormal vectors perpendicular to p, and $\phi : \mathbb{R}^3 \to \mathbb{R}^+$ is large near the boundary of differing diffusion regions, e.g.,

$$\phi(x) = \frac{1}{|B(x, R)|} \int_{B(x,R)} \|I(y, \cdot) - \mu_{B(x,R)}(\cdot)\|^2 \, \mathrm{d}y \tag{9}$$

where $B(x,R)$ is the ball centered at x of chosen radius R, $|B(x,R)|$ denotes the volume, and the norm is defined as in (7). For this choice of potential, we are interested in *maximizing* the corresponding energy. The objective is to initialize the tubular surface inside the CB, and then increase surface area until the surface reaches the boundary of differing diffusion patterns.

4 Energy Optimization

In this section, we construct a steepest descent flow to minimize the energy of interest (3). A steepest descent is considered since we are not necessarily interested in the global maximizer or minimizer; indeed, the energy corresponding to (8) does not have a global maximizer. We begin with a tubular surface initialization (see Section 5 for the procedure), i.e., an initial 4D curve, and follow the gradient or its opposite depending on the whether we want to maximize or minimize the energy.

4.1 Gradient Descent: Fixed Endpoints

The standard technique for calculating the gradient of an energy defined on curves, which is based on a geometrized $\mathbb{L}^2$ metric on the space of curves, cannot be applied to our energy of interest. This is because of the fact that when minimizing (3) using $\mathbb{L}^2$, Ψ must satisfy a certain positivity condition (see [22]) that we cannot guarantee for our choices of Ψ otherwise the gradient descent is ill-posed. Moreover, when maximizing (3), we are indeed maximizing a weighted length, which with respect to the standard geometrized $\mathbb{L}^2$ curve metric, leads to an *unstable reverse diffusion*. As shown in [23], such weighted length functionals may be optimized in a *stable* manner by moving in the gradient direction of the energy (3) with respect to a *geometrized Sobolev metric*:

Definition 1. *Let $\tilde{c} : [0,1] \to \mathbb{R}^4$ be such that $\tilde{c}(0)$, $\tilde{c}(1)$ are fixed. Let $h, k : [0,1] \to \mathbb{R}^4$ be perturbations of $\tilde{c}$ then*

$$\langle h, k \rangle_{\mathbb{L}^2} := \frac{1}{L} \int_{\tilde{c}} h(\tilde{s}) \cdot k(\tilde{s}) \, \mathrm{d}\tilde{s},$$
$$\langle h, k \rangle_{\text{Sob}} := L \int_{\tilde{c}} h'(\tilde{s}) \cdot k'(\tilde{s}) \, \mathrm{d}\tilde{s},$$

where L is the length of of the curve $\tilde{c}$, $\mathrm{d}\tilde{s}$ is arclength element of $\tilde{c}$, and the derivatives are with respect to the arclength parameter $\tilde{s}$.

It can be shown that the gradient of (3) with respect to the Sobolev metric above is

$$\frac{1}{L} \nabla_{\text{Sob}} E(\tilde{c}) = K(\Psi_{\tilde{p}}) + \partial_{\tilde{s}} K(\hat{\Psi}_v \sqrt{1 + (r_{\tilde{s}}/|c_{\tilde{s}}|)^2} + \Psi \tilde{c}_{\tilde{s}}), \tag{10}$$

where

$$K(f) := \int_0^L K(\cdot, \tilde{s}) f(\tilde{s}) \, \mathrm{d}\tilde{s}, \quad K(\tilde{s}_1, \tilde{s}_2) = \frac{1}{L} \begin{cases} \frac{\tilde{s}_2}{L}(1 - \frac{\tilde{s}_1}{L}) & 0 \le \tilde{s}_2 \le \tilde{s}_1 \\ \frac{\tilde{s}_1}{L}(1 - \frac{\tilde{s}_2}{L}) & \tilde{s}_1 \le \tilde{s}_2 \le L \end{cases}. \tag{11}$$

The expression has the additional numerical advantage that only first order derivatives are required in comparison to the standard $\mathbb{L}^2$ gradient, which needs second order information, and simply cannot be used anyway since it results in an unstable flow. Note that as stated in [23], the expression (10) may be computed efficiently in order N complexity, where N is the number of sample points of the curve.

4.2 Evolving Endpoints

In the previous subsection, we derived a gradient descent flow for (3) provided the endpoints of the $4D$ curve (i.e., the end cross sections of the tube) are fixed. We now describe how to evolve the endpoints so as to reduce the energy. This is useful for some choices of Ψ in (3), for example, Ψ_2 defined in (8). To determine the evolution of the endpoints, we compute the variation with respect to the endpoints. This results in

$$\tilde{c}_t(0) = \mp\hat{\Psi}_v\sqrt{1+\left(\frac{r_{\tilde{s}}}{|c_{\tilde{s}}|}\right)^2} \mp \Psi\tilde{c}_{\tilde{s}},\ \tilde{c}_t(1) = \pm\hat{\Psi}_v\sqrt{1+\left(\frac{r_{\tilde{s}}}{|c_{\tilde{s}}|}\right)^2} \pm \Psi\tilde{c}_{\tilde{s}}, \qquad (12)$$

which will minimize/maximize the energy (depending on the sign chosen above). Therefore, the algorithm to reduce the energy is to alternatively evolve the endpoints by (12) and then evolve the 4D curve by (10).

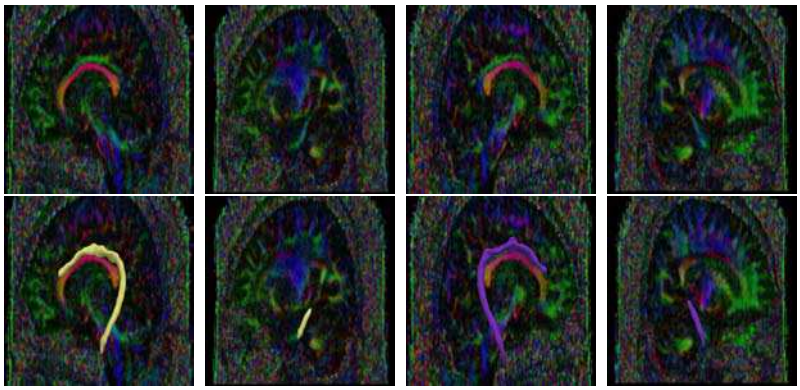

Fig. 2. Selected slice-wise views of CB Segmentation results from proposed framework. The top row shows the DWI data and the bottom row shows the DWI data with the extracted surface rendered in 3D.

5 Experiments and Results

The algorithm was applied to DWI data of the brain from a data set that included schizophrenic and normal control subjects, with the DWI being acquired for 54 sampling directions. Results are included for the data from 2 subjects, and show the CB extracted for both the right and left bundles in each case.

In this paper, a perturbation of the anchor tract is used as the initial centerline curve and the smallest possible radius of 0.5 is used, with the surface essentially growing out from this initial radius. There are also other options to perform this initialization. Since we are given seed regions determined by an expert, an alternative initialization would be to connect the two seed regions with a streamline that passed above the Corpus Callosum (which is easy to segment). This initialization is being explored for future work.

The results included in this paper show the application of the proposed framework to the data sets, using the energy (3) using the potential Ψ_1 (4). Figure 2 shows slice-wise

views of the CB segmentation results obtained from the proposed framework indicating the homogeneity of the discs within the captured volume. The Figures, 3, and 4 show the tubular surface extracted by the proposed algorithm. It is to be noted that the surfaces are accurate while the boundaries shown in Figure 2 are the boundary locations rounded off to the grid points by the visualization process.

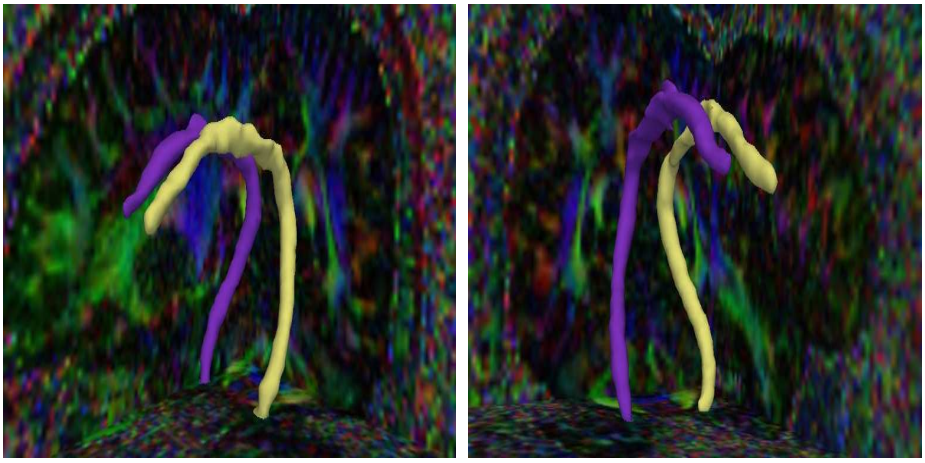

Fig. 3. CB Segmentation Results for Brain data set 1. Yellow shows the left CB and magenta shows the right CB.

6 Conclusions and Future work

We have proposed a novel technique to extract the cingulum bundle, which is of interest in the medical community because of its ties to schizophrenia, from DW-MRI of the brain. Unlike other standard techniques for extracting fiber bundles in the brain, we are able to *extract the entire bundle as a region at once rather* than detecting individual fibers and then combining them to form the bundle, which is laborious and prone to errors, while also performing this as a curve evolution rather than a surface evolution thus avoiding the computational disadvantages of a levelset implementation. We have *modeled the cingulum bundle as a tubular surface* and constructed a variational approach to detect the optimum tubular surface from DW-MRI, which represents the CB. Tubular surfaces provide a natural and accurate *shape prior* for the cingulum bundle, and such a shape prior is necessary due to the noisy nature of the imagery and the fact that data is not very visible or highly corrupted in certain slices. As we have shown, the tubular surface can be represented as a 4D curve, and thus, we were able to *significantly reduce the computational cost* of the algorithm compared to extracting an arbitrary surface. The proposed model was shown to yield good segmentations of the Cingulum Bundle upon visual inspection; unfortunately, there is no expert ground truth data available since it is laborious to hand segment an entire volume and certain slices do not even display the CB diffusion pattern accurately.

In future work, the authors plan to explore different choices of Ψ in the energy functional(3), and explore smoothness terms for the tubes in the energy. We will also

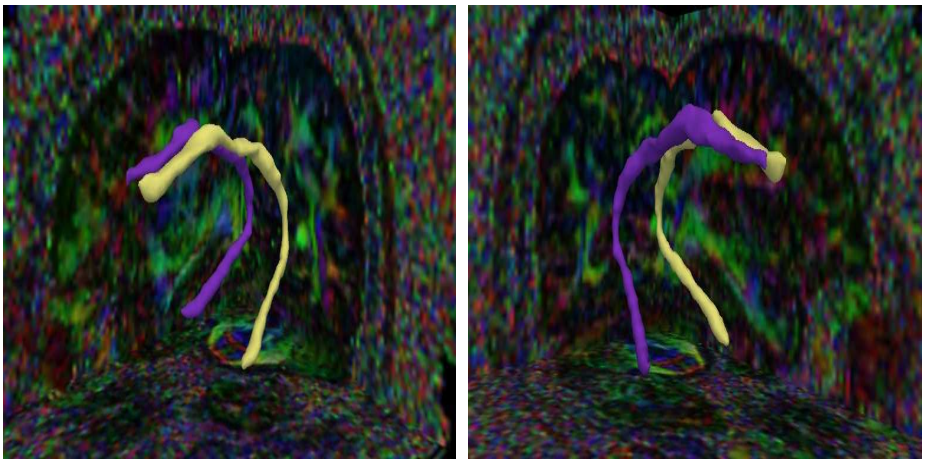

Fig. 4. CB Segmentation Results for Brain data set 2. Yellow shows the left CB and magenta shows the right CB.

implement the evolution of endpoints, which will be useful since the initialization will have to only be a single seed point. Further, the use of the extracted Cingulum Bundles will be explored in population studies for the discrimination of Schizophrenia. We are also interested in applying the framework other tubular structures such as the Uncinate Fasciculus in the brain.

This work was supported in part by grants from NSF, AFOSR, ARO, MURI, as well as by a grant from NIH (NAC P41 RR-13218) through Brigham and Women's Hospital. This work is part of the National Alliance for Medical Image Computing (NAMIC), funded by the National Institutes of Health through the NIH Roadmap for Medical Research, Grant U54 EB005149. Information on the National Centers for Biomedical Computing can be obtained from *http://nihroadmap.nih.gov/bioinformatics*.

References

1. Kubicki, M., Westin, C., Nestor, P., Wible, C., Frumin, M., Maier, S., Kikinis, R., Jolesz, F., McCarley, R., Shenton, M.: Cingulate fasciculus integrity disruption in schizophrenia: a magnetic resonance diffusion tensor imaging study. Biological Psychiatry **54**(11) (2003) 1171–1180
2. Wang, F., Sun, Z., Cui, L., Du, X., Wang, X., Zhang, H., Cong, Z., Hong, N., Zhang, D.: Anterior Cingulum Abnormalities in Male Patients With Schizophrenia Determined Through Diffusion Tensor Imaging (2004)
3. Mori, S., Crain, B., Chacko, V., van Zijl, P.: Three dimensional tracking of axonal projections in the brain by magnetic resonance imaging. Ann. of Neurol. **45**(2) (1999) 265–269
4. Conturo, T., Lori, N., Cull, T., Akbudak, E., Snyder, A., Shimony, J., McKinstry, R., Burton, H., Raichle, M.: Tracking neuronal fiber pathways in the living human brain. Proc. Natl. Acad. Sci USA **96**(18) (1999) 10422–10427

5. Perrin, M., Poupon, C., Cointepas, Y., Rieul, B., Golestani, N., Pallier, C., Rivière, D., Constantinesco, A., Bihan, D.L., Mangin, J.F.: Fiber tracking in q-ball fields using regularized particle trajectories. [24] 52–63
6. Parker, G.J.M., Wheeler-Kingshott, C.A.M., Barker, G.J.: Estimating distributed anatomical brain connectivity using fast marching methods and diffusion tensor imaging. IEEE Trans. Med. Imaging **21**(5) (2002) 505–512
7. Friman, O., Farnebäck, G., Westin, C.F.: A bayesian approach for stochastic white matter tractography. IEEE Trans. Med. Imaging **25**(8) (2006) 965–978
8. Lenglet, C., Rousson, M., Deriche, R., Faugeras, O.D., Lehericy, S., Ugurbil, K.: A riemannian approach to diffusion tensor images segmentation. [24] 591–602
9. Control Theory and Fast Marching Techniques for Brain Connectivity Mapping. In: CVPR (1). (2006)
10. Zhang, F., Goodlett, C., Hancock, E.R., Gerig, G.: Probabilistic fiber tracking using particle filtering. In Ayache, N., Ourselin, S., Maeder, A.J., eds.: MICCAI (2). Volume 4792 of Lecture Notes in Computer Science., Springer (2007) 144–152
11. Cohen-Adad, J., Descoteaux, M., Rossignol, S., Hoge, R.D., Deriche, R., Benali, H.: Detection of multiple pathways in the spinal cord white matter using q-ball imaging. In: IEEE International Symposium on Biomedical Imaging : From Nano to Macro. (2008)
12. Xu, C., Pham, D.L., Prince, J.L.: Finding the brain cortex using fuzzy segmentation, isosurfaces, and deformable surface models. In Duncan, J.S., Gindi, G., eds.: IPMI. Volume 1230 of Lecture Notes in Computer Science., Springer (1997) 399–404
13. Yezzi, A.J., Kichenassamy, S., Kumar, A., Olver, P.J., Tannenbaum, A.: A geometric snake model for segmentation of medical imagery. IEEE Trans. Med. Imaging **16**(2) (1997) 199–209
14. Lenglet, C., Rousson, M., Deriche, R.: Dti segmentation by statistical surface evolution. IEEE Trans. Med. Imaging **25**(6) (2006) 685–700
15. Wang, Z., Vemuri, B.C.: Dti segmentation using an information theoretic tensor dissimilarity measure. IEEE Trans. Med. Imaging **24**(10) (2005) 1267–1277
16. Awate, S.P., 0005, H.Z., Gee, J.C.: Fuzzy nonparametric dti segmentation for robust cingulum-tract extraction. In Ayache, N., Ourselin, S., Maeder, A.J., eds.: MICCAI (1). Volume 4791 of Lecture Notes in Computer Science., Springer (2007) 294–301
17. Melonakos, J., Mohan, V., Niethammer, M., Smith, K., Kubicki, M., Tannenbaum, A.: Finsler tractography for white matter connectivity analysis of the cingulum bundle. In: MICCAI (1). (2007) 36–43
18. Melonakos, J., Niethammer, M., Mohan, V., Smith, K., Kubicki, M., Tannenbaum, A.: Locally-constrained region-based methods for dw-mri segmentation. In: MMBIA. (2007)
19. Li, H., Yezzi, A.: Vessels as 4-d curves: Global minimal 4-d paths to extract 3-d tubular surfaces and centerlines. IEEE Transactions on Medical Imaging **26**(9) (2007) 1213–1223
20. Cohen, L.D., Kimmel, R.: Global minimum for active contour models: A minimal path approach. In: CVPR, IEEE Computer Society (1996) 666–673
21. Schmahmann, J., Pandya, D.: Fiber Pathways of the Brain. Oxford University Press (2006)
22. Melonakos, J., Pichon, E., Angenent, S., Tannenbaum, A.: Finsler active contours. IEEE Transactions on Pattern Analysis and Machine Intelligence (To Appear)
23. Sundaramoorthi, G., Yezzi, A.J., Mennucci, A., Sapiro, G.: New possibilities with Sobolev active contours. In: SSVM. (2007) 153–164
24. Christensen, G.E., Sonka, M., eds.: Information Processing in Medical Imaging, 19th International Conference, IPMI 2005, Glenwood Springs, CO, USA, July 10-15, 2005, Proceedings. In Christensen, G.E., Sonka, M., eds.: IPMI. Volume 3565 of Lecture Notes in Computer Science., Springer (2005)